

# Mermin-Wagner physics, $(H, T)$ phase diagram, and candidate quantum spin-liquid phase in the spin-1/2 triangular-lattice antiferromagnet $\text{Ba}_8\text{CoNb}_6\text{O}_{24}$

Y. Cui,<sup>1</sup> J. Dai,<sup>1</sup> P. Zhou,<sup>1</sup> P. S. Wang,<sup>1</sup> T. R. Li,<sup>1</sup> W. H. Song,<sup>1</sup> J. C. Wang,<sup>1</sup> L. Ma,<sup>2</sup> Z. Zhang,<sup>3</sup> S. Y. Li,<sup>3,4</sup> G. M. Luke,<sup>5,6</sup> B. Normand,<sup>7</sup> T. Xiang,<sup>8,9</sup> and W. Yu<sup>1,\*</sup>

<sup>1</sup>*Department of Physics and Beijing Key Laboratory of Opto-electronic Functional Materials & Micro-nano Devices, Renmin University of China, Beijing, 100872, China*

<sup>2</sup>*High Magnetic Field Laboratory, Chinese Academy of Sciences, Hefei 230031, China*

<sup>3</sup>*State Key Laboratory of Surface Physics and Laboratory of Advanced Materials, Department of Physics, Fudan University, Shanghai 200433, China*

<sup>4</sup>*Collaborative Innovation Center of Advanced Microstructures, Nanjing 210093, China*

<sup>5</sup>*Department of Physics and Astronomy, McMaster University, Hamilton L8S 4M1, Canada*

<sup>6</sup>*Canadian Institute for Advanced Research, Toronto M5G 1Z8, Canada*

<sup>7</sup>*Neutrons and Muons Research Division, Paul Scherrer Institute, CH-5232 Villigen-PSI, Switzerland*

<sup>8</sup>*Institute of Physics, Chinese Academy of Sciences, Beijing 100190, China*

<sup>9</sup>*Collaborative Innovation Center of Quantum Matter, Beijing 100190, China*

$\text{Ba}_8\text{CoNb}_6\text{O}_{24}$  presents a system whose  $\text{Co}^{2+}$  ions have an effective spin 1/2 and construct a regular triangular-lattice antiferromagnet (TLAFM) with a very large interlayer spacing, ensuring purely two-dimensional character. We exploit this ideal realization to perform a detailed experimental analysis of the  $S = 1/2$  TLAFM, which is one of the keystone models in frustrated quantum magnetism. We find strong low-energy spin fluctuations and no magnetic ordering, but a diverging correlation length down to 0.1 K, indicating a Mermin-Wagner trend towards zero-temperature order. Below 0.1 K, however, our low-field measurements show an unexpected magnetically disordered state, which is a candidate quantum spin liquid. We establish the  $(H, T)$  phase diagram, mapping in detail the quantum fluctuation corrections to the available theoretical analysis. These include a strong upshift in field of the maximum ordering temperature, qualitative changes to both low- and high-field phase boundaries, and an ordered regime apparently dominated by the collinear “up-up-down” state.  $\text{Ba}_8\text{CoNb}_6\text{O}_{24}$  therefore offers fresh input for the development of theoretical approaches to the field-induced quantum phase transitions of the  $S = 1/2$  Heisenberg TLAFM.

## I. Introduction

The challenge of frustrated quantum magnetism now extends from theory and numerics through experiment to materials synthesis. This challenge is to characterize and to understand the effects of quantum spin fluctuations in dimensions greater than 1. In two dimensions (2D), where the  $S = 1/2$  square-lattice antiferromagnet (SLAFM) with Heisenberg interactions has clear magnetic order with a suppressed moment ( $m_s \simeq 0.61m_0$ , where  $m_0$  is the full moment) and the kagome-lattice AFM has no order at all, the triangular-lattice antiferromagnet (TLAFM) lies close to the boundary where the frustration-driven quantum fluctuations are sufficient to destroy  $m_s$ . While this situation has led to a range of exotic proposals for the ground state of the Heisenberg TLAFM [1–4], detailed studies have demonstrated that the true ground state does in fact have a finite semiclassical magnetic order, in a noncollinear  $120^\circ$  structure [5, 6], with a best estimate for  $m_s$  of  $0.41m_0$  [7].

Nevertheless, the strong frustration of the TLAFM leads to an extensive renormalization of physical properties at all energy scales. As a consequence, the dynamical and thermodynamic properties of the TLAFM have

remained as a long-standing conundrum due to the inadequacy of theoretical approximations, the limitations of numerical approaches (including small system sizes in exact diagonalization, the minus-sign problem in quantum Monte Carlo, and the 1D restriction on density-matrix renormalization-group (DMRG) methods), and the absence of pure 2D systems for experimental investigation. A full understanding of the TLAFM would also aid the understanding of other exotic quantum states, most notably spin liquids [8], unconventional superconductors [9], and systems with complex magnetic order [10], in all of which geometric frustration has an essential role.

Purely 2D models such as the TLAFM are difficult to realize in the 3D world, and a further complication to experiment is that their physics is controlled by the Mermin-Wagner theorem [11], which describes the dominant effects of additional thermal fluctuations in the restricted phase space of a low-dimensional system. Specifically, the theorem dictates that in 2D a continuous symmetry can be broken, allowing a finite order parameter, only at exactly zero temperature. In practice, most experimental systems are subject to a weak 3D coupling that stabilizes their semiclassical order, and so examples of “Mermin-Wagner order,” meaning incipient order as  $T \rightarrow 0$ , are rare.

Among the known compounds approximating the spin-1/2 TLAFM [12, 13], the materials  $\text{Ba}_3\text{CoSb}_2\text{O}_9$  and  $\text{Ba}_3\text{CoNb}_2\text{O}_9$  have attracted particular attention. They

\* wqyu\_phy@ruc.edu.cn

have perfectly regular lattices of  $\text{Co}^{2+}$  ions and preserve inversion symmetry close to the plane, so that any Dzyaloshinskii-Moriya interactions are too weak to break the continuous symmetry [14–18]. The exchange interactions are found to be close to the pure Heisenberg form, albeit with a weak anisotropy ( $J_x = J_y \neq J_z$ ). Magnetic order occurs at finite temperatures due to weak inter-plane coupling, which releases the stricture of the 2D Mermin-Wagner theorem. The rich variety of competing magnetically ordered phases at finite applied magnetic fields [10, 17] provides evidence of the expected frustration effects. Available theoretical approaches [19–23] suggest the presence of low-lying and weakly dispersive excitations, which were observed only recently in  $\text{Ba}_3\text{CoSb}_2\text{O}_9$  [24], and whose effects on the thermodynamic properties of the TLAFM lie beyond the semiclassical predictions of the nonlinear  $\sigma$  model [23, 25, 26].

Here we take an experimental approach to the physical properties of the spin-1/2 TLAFM close to the Heisenberg point, which hinges on the remarkable properties of the dielectric compound  $\text{Ba}_8\text{CoNb}_6\text{O}_{24}$ . This system has regular triangular layers of effectively low-spin  $\text{Co}^{2+}$  ions separated by a very large interlayer spacing,  $c \simeq 18.9$  Å [27], which ensures that, from a magnetic point of view, it is ideally 2D. It has been argued very recently by analyzing bulk thermodynamic measurements that the magnetic Hamiltonian is that of an ideal TLAFM with only Heisenberg interactions [28]. Here we combine magnetization,  $g$ -factor, susceptibility, specific-heat, and  $^{93}\text{Nb}$  nuclear quadrupole and magnetic resonance (NQR and NMR) measurements down to temperatures of 0.028 K, to show that above 0.1 K  $\text{Ba}_8\text{CoNb}_6\text{O}_{24}$  provides a nearly ideal experimental illustration of textbook Mermin-Wagner physics in a 2D magnetic system. However, below 0.1 K our NQR and NMR data reveal an anomalous suppression of low-energy spin fluctuations, breaking the trend towards zero-temperature magnetic order. Instead they indicate a disordered phase, possibly a quantum spin liquid (QSL), at zero field, and at finite fields and temperatures an anomalously broad regime of apparent collinear “up-up-down” polarization.

The structure of this paper is as follows. In Sec. II we present the material and experimental methods, with which we first establish that the system has an effective spin  $S = 1/2$  and a nearest-neighbor AFM exchange coupling  $J \simeq 1.66$  K. In Sec. III we show our results for the low-temperature ( $T > 0.08$  K) susceptibility and specific heat, and illustrate briefly how these thermodynamic quantities provide a semi-quantitative validation of available theoretical (series-expansion and Schwinger-boson) approaches to the TLAFM. Section IVA presents our NQR data, which confirm the lack of spontaneous magnetization down to 0.028 K at zero field, but with a correlation length that increases steeply upon cooling to 0.1 K, and then quantify the departures from Mermin-Wagner behavior below this temperature. In Sec. IVB we show our NMR results for the spectrum and spin-lattice relaxation rate, which we compile as a field-temperature

phase diagram. In Sec. V we discuss the interpretation of these results in terms of quantum corrections to the classical phase diagram, accompanied by the appearance of the unexpected candidate QSL phase at low field and temperature. In Sec. VI we provide a short summary.

## II. Material and Methods

Polycrystalline  $\text{Ba}_8\text{CoNb}_6\text{O}_{24}$  samples were synthesized by a solid-state reaction method [27]. For structural characterization we performed powder x-ray diffraction measurements and made a complete Rietveld refinement using the Fullprof package. The material crystallizes in the space group  $P\bar{3}m1$ , illustrated in Fig. 1(a).  $\text{Co}^{2+}$  ions in  $\text{CoO}_6$  octahedra form a corner-sharing geometry with  $\text{NbO}_6$  octahedra, constructing perfect layers of regular triangular lattices [Fig. 1(b)], with neighboring  $\text{Co}^{2+}$  planes separated by eight  $\text{Ba}^{2+}$  and six  $\text{NbO}_6$  layers. The lattice parameters [27] are  $a = 5.789813$  Å, which is almost identical to  $\text{Ba}_3\text{CoNb}_2\text{O}_9$  ( $a = 5.7737$  Å), but  $c = 18.89355$  Å, which is approximately three times longer.

Our comprehensive experimental analysis of  $\text{Ba}_8\text{CoNb}_6\text{O}_{24}$  combines magnetization,  $g$ -factor, susceptibility, specific-heat, NQR, and NMR measurements. Magnetization and susceptibility data were measured in a PPMS-VSM for temperatures  $T > 2$  K and in a  $^3\text{He}$  SQUID system for  $0.6$  K  $< T < 1.8$  K. The temperature-dependent  $g$ -factors were obtained by field-sweep electron spin resonance (ESR) at a fixed frequency 9.397 GHz. The specific heat was measured in a PPMS dilution refrigerator (DR), which reached temperatures down to 0.08 K. The  $^{93}\text{Nb}$  ( $I = 9/2$ ) NQR signal was detected by the spin-echo technique in a DR system reaching temperatures down to 0.028 K. Temperatures in both NQR and NMR were read from a  $\text{RuO}_2$  thermometer and verified using the  $^{63}\text{Cu}$  NMR echo intensity of the coil, which is inversely proportional to the temperature. The NMR spin-lattice relaxation rate,  $1/^{93}T_1$ , was determined by the magnetization inversion-recovery method, with the spin recovery, which showed no stretching behavior, fitted by the standard  $I = 9/2$  functions  $m(t) = m(\infty) - a[0.121e^{-3t/T_1} + 0.56e^{-10t/T_1} + 0.297e^{-21t/T_1} + 0.022e^{-36t/T_1}]$  for NQR and  $m(t) = m(\infty) - a[0.152e^{-t/T_1} + 0.14e^{-6t/T_1} + 0.153e^{-15t/T_1} + 0.192e^{-28t/T_1} + 0.363e^{-45t/T_1}]$  for the NMR lines [29, 30]. Theoretical values for the thermodynamic quantities  $\chi(T)$ ,  $C_m(T)$ , and  $S_m(T)$  were digitized from the cited literature and scaled appropriately.

It is necessary first to establish the effective spin of the  $\text{Co}^{2+}$  ions in  $\text{Ba}_8\text{CoNb}_6\text{O}_{24}$ . Figure 1(c) shows the magnetization,  $M$ , as a function of field at a fixed temperature  $T = 0.46$  K.  $M$  increases rapidly, from exactly zero field and completely linearly, up to a field  $H_s = 3.00 \pm 0.04$  T; at this temperature there is no evidence for a feature at 1/3 magnetization, to which we return in Sec. IV. Beyond  $H_s$ , a weak linear increase is

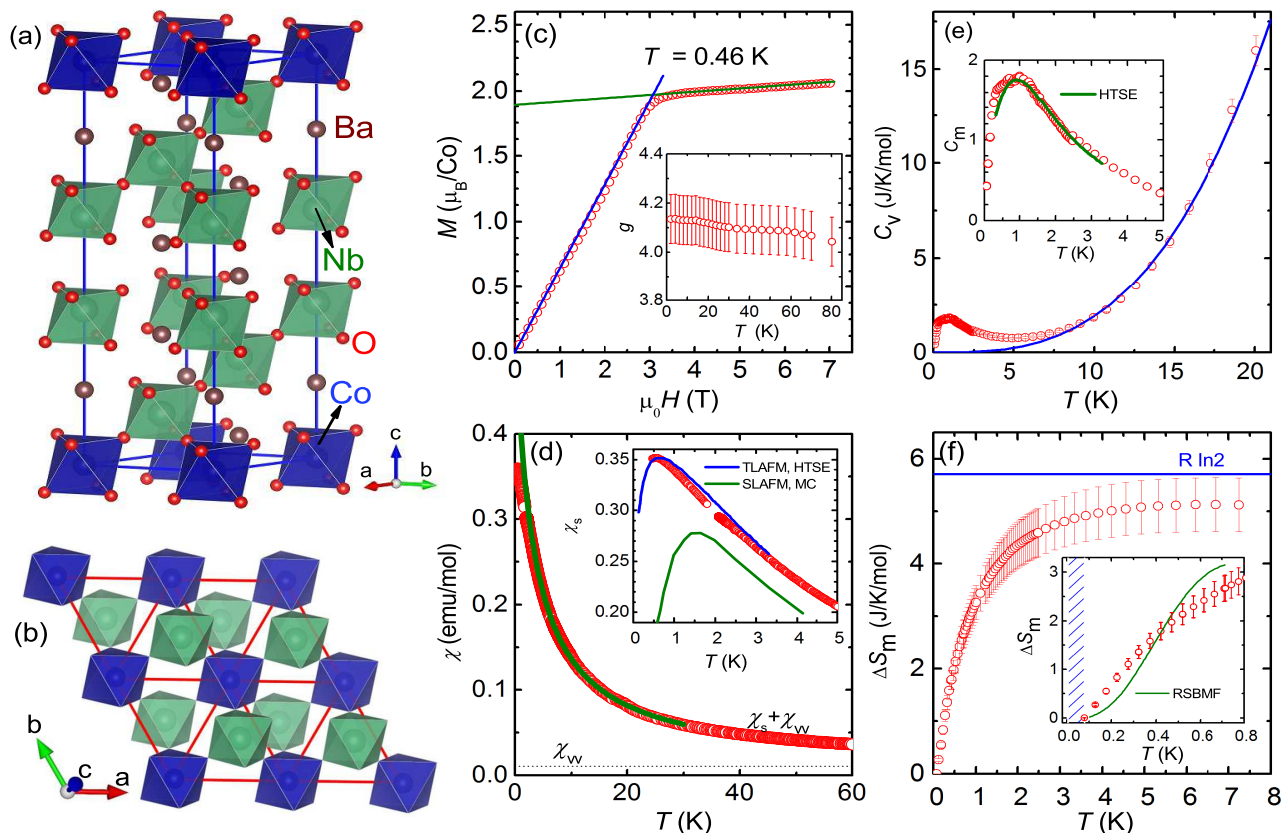


FIG. 1. **Lattice structure and magnetic properties of  $\text{Ba}_3\text{CoNb}_6\text{O}_{24}$ .** (a) The triangular-lattice planes formed from the  $\text{CoO}_6$  units are separated by many nonmagnetic units, specifically 8  $\text{Ba}^{2+}$  and 6  $\text{NbO}_6$  layers. (b) A plane of  $\text{CoO}_6$  octahedra, showing their triangular-lattice configuration and the neighboring, corner-sharing  $\text{NbO}_6$  octahedra that mediate the antiferromagnetic interactions. (c) Magnetization,  $M$ ; blue and green straight lines represent linear fits to the low- and high-field data, whose origins lie respectively in the effective-spin and van Vleck paramagnetic contributions. Inset:  $g$ -factor as a function of temperature. (d) dc susceptibility measured under a field of 0.1 T. The solid green line is a fit to a Curie-Weiss form,  $\chi_s(T) = a/(T + \theta)$ , combined with an offset of  $\chi_{vv}$ , the constant van Vleck contribution determined from  $M$ . The fitting parameters for the low-temperature regime are  $a = 1.7$  emu K/mol and  $\theta = 3.5 \pm 0.5$  K. Inset: low-temperature spin susceptibility; the blue line shows HTSE results for the Heisenberg TLAFM, adapted from Ref. [25]; the green line shows Monte Carlo results for the Heisenberg SLAFM, adapted from Ref. [34]. Both curves use the parameters  $J = 1.66$  K and  $g = 4.13$ . (e) Specific heat at zero field. The solid line is a fit to  $C_v = bT^3$ . Inset: low-temperature magnetic specific heat,  $C_m$ , after subtracting the phonon contribution; the green line is the HTSE result for the Heisenberg TLAFM, adapted from Ref. [25] with  $J = 1.66$  K. (f) Magnetic entropy,  $S_m(T)$ , obtained by integrating the specific-heat data above 0.08 K. The solid line shows the high-temperature limit,  $S_m(\infty) = R \ln(2S + 1)$  in a spin- $S$  system, for  $S = 1/2$ . Inset: low-temperature magnetic entropy, showing for comparison RSBMF results (see text) adapted from Ref. [23] with  $J = 1.66$  K. Blue shading represents the temperature region excluded from our analysis.

also observable, which can be ascribed to van Vleck paramagnetism [17].  $H_s$  is the saturation field required to polarize fully the magnetic moment of  $\text{Co}^{2+}$ , as also measured for  $\text{Ba}_3\text{CoSb}_2\text{O}_9$  [14–16] and  $\text{Ba}_3\text{CoNb}_2\text{O}_9$  [17, 18]. The saturation moment of the  $\text{Co}^{2+}$  ions deduced from Fig. 1(c) is  $m_s = 1.92 \pm 0.1\mu_B$ . ESR measurements of the  $g$ -factor at different temperatures, shown in the inset of Fig. 1(c), approach a constant value,  $g = 4.13 \pm 0.1$ , below 20 K. The effective spin of the  $\text{Co}^{2+}$  ions is therefore  $m_s/g\mu_B \simeq 0.464$ , which is consistent with spin-1/2. This is the result expected from the crystal-field analysis for  $\text{Co}^{2+}$  in an octahedral environment with a weak trigonal distortion [14, 31], where the relatively strong

spin-orbit coupling leads to the formation of six nondegenerate Kramers doublets and hence to an effective spin  $S = 1/2$  with a large  $g$ -factor at low temperatures.

The magnetic exchange coupling can be estimated from the same data. From the corner-sharing geometry of neighboring  $\text{CoO}_6$  and  $\text{NbO}_6$  octahedra, the dominant magnetic interactions between in-plane  $\text{Co}^{2+}$  spins occur by Co-O-O-Co and Co-O-Nb-O-Co superexchange couplings [17]; the very long paths make the interaction strength extremely sensitive to geometrical details and should preclude all but nearest-neighbor couplings. For the effective  $S = 1/2$   $\text{Co}^{2+}$  ions, one expects an XXZ spin model of the form  $H = \sum_{\langle ij \rangle} J_x(S_i^x S_j^x + S_i^y S_j^y) + J_z S_i^z S_j^z$ ,

where  $\langle ij \rangle$  denotes only nearest-neighbor spins [14–18]. In  $\text{Ba}_3\text{CoSb}_2\text{O}_9$ , the exchange coupling was stated initially to be nearly isotropic (Heisenberg), with  $J_x = J_y \approx J_z \approx 18.2$  K [14–16], but has since been found to have easy-plane character ( $J_z/J_x \simeq 0.89$ ) [24]. In  $\text{Ba}_3\text{CoNb}_2\text{O}_9$ , double magnetic transitions at 1.36 K and 1.10 K in zero field indicate a weak easy-axis anisotropy,  $J_z > J_x$  [17, 18, 32, 33], with  $J_x$  of order 2 K.

Because  $\text{Ba}_8\text{CoNb}_6\text{O}_{24}$  and  $\text{Ba}_3\text{CoNb}_2\text{O}_9$  have an almost identical planar structure, very similar exchange couplings are expected. It is tempting to estimate the exchange directly from the magnetization [Fig. 1(c)], which by using the result  $g\mu_B H_s = 4.5J$  for the Heisenberg TLAFM at  $T = 0$  [10] yields  $J = 1.84 \pm 0.10$  K. However, this procedure has the weakness that our measurement of  $M$  is not made at zero temperature, which turns out to be a source of significant inaccuracy due to the complex low-temperature physics of  $\text{Ba}_8\text{CoNb}_6\text{O}_{24}$ . We use instead the result from our NMR measurements at 0.028 K,  $H_s = 2.7 \pm 0.1$  T (Sec. IV), which yields  $J = 1.66 \pm 0.06$  K. This result is fully consistent with the very recent estimate of Ref. [28], which was made on the basis of comparison with thermodynamic properties (Sec. III).

### III. Thermodynamic Properties

The dc susceptibility,  $\chi(T)$ , of the sample, measured under a field of 0.1 T, is shown in Fig. 1(d).  $\chi(T)$  increases monotonically on cooling down to 1 K and can be separated into two contributions,  $\chi(T) = \chi_{vv} + \chi_s(T)$ , where  $\chi_{vv} \simeq 0.019\mu_B/\text{Co}/\text{T}$ , or 0.0106 emu/mol, is the van Vleck paramagnetic contribution determined from the magnetization [Fig. 1(c)].  $\chi_s(T)$  follows an approximate Curie-Weiss (CW) form,  $\chi_s(T) = a/(T + \theta)$ , which represents the average contribution of the coupled  $\text{Co}^{2+}$  spins. In the low-temperature regime ( $T < 30$  K), we obtain a Weiss constant  $\theta = 3.5 \pm 0.5$  K. From the constant of proportionality,  $a = 1.7$  emu K/mol, we deduce an effective moment  $\mu_{\text{eff}} = 3.69\mu_B$ , which is fully consistent with our determination of the saturation moment,  $m_s$  (Sec. II), because of the value of the  $g$ -factor. These results are quantitatively consistent with those of Ref. [28], and also with the results of Ref. [17] for  $\text{Ba}_3\text{CoNb}_2\text{O}_9$ . At low temperatures,  $T \lesssim J$ ,  $\chi_s(T)$  is expected to fall below the CW form as the spins become correlated, giving the characteristic broad maximum revealed by numerical approaches to the  $S = 1/2$  TLAFM. In the inset of Fig. 1(d), we compare our data with the results for  $\chi_s(T)$  obtained by the high-temperature series-expansion (HTSE) method applied to the Heisenberg TLAFM, adapted from Ref. [25] using the parameters  $J = 1.66$  K and  $g = 4.13$ . The HTSE result and experimental measurements are quantitatively consistent.

We stress that this comparison is not a fit, because with  $J$  and  $g$  fixed there are no free parameters. While a best fit to the peak position would return a smaller  $J$  value, as noted above we rely on our measurement of the

low- $T$  saturation field to determine  $J$ . The errors in the measured susceptibility arise from the sample mass (3%), the determination of the  $g$ -factor (3%), and the accuracy of the SQUID data from the VSM (5%). In this context, the fact that our data and HTSE agree within 2.5% at all temperatures constitutes full agreement.

We draw attention to the generic property of the TLAFM that the peak in  $\chi_s(T)$  occurs at the anomalously low temperature  $T \approx 0.4J$ ; this direct consequence of frustration can be contrasted with the behavior of the unfrustrated SLAFM, adapted from Ref. [34] and also shown in the inset of Fig. 1(d), where the peak appears at  $T \approx J$ . HTSE is by nature an approach from high temperatures, which reaches its limits at the unusually low temperatures of the  $\chi_s$  peak in the TLAFM, and its use requires careful choice of representative Padé approximants. Thus this degree of consistency offers a benchmark both for the capabilities of HTSE and for the degree to which  $\text{Ba}_8\text{CoNb}_6\text{O}_{24}$  offers an ideal 2D  $S = 1/2$  Heisenberg TFAFM.

Further valuable thermodynamic information is provided by the specific heat,  $C_v(T)$ , shown in Fig. 1(e). The absence of any sharp peak or cusp in  $C_v$  suggests that magnetic ordering is absent to the lowest temperature (80 mK) we can access in this measurement. Because  $C_v$  falls rapidly from 20 K to 7.5 K, following an exact  $T^3$  behavior, we use this to subtract the presumed phonon contribution and isolate the magnetic specific heat,  $C_m(T)$ . This procedure can be followed with a high degree of confidence because the characteristic energy scales of the phonons are manifestly very high compared to the magnon contributions in this system, which peak at 1 K. However, we caution that even very small residual uncertainties may be important in the entropy analysis below, and contribute to the error bars we display.  $C_m(T)$ , shown in the inset of Fig. 1(e), confirms the absence of ordering features, is dominated by a broad peak at  $T \approx 1.0$  K, and below 0.3 K falls rapidly towards  $C_m = 0$ . While its shape over the available data range shows no evidence for an activated form, a detailed inspection at the lowest temperatures sets an upper limit of approximately 0.05 K on any possible spin gap. Once again we compare our data with the HTSE result [25] for the Heisenberg TLAFM with  $J = 1.66$  K, finding near-perfect quantitative agreement over the available range of the HTSE data ( $0.3 \text{ K} \leq T \leq 2.5 \text{ K}$ ). As for the susceptibility, the peak in  $C_m(T)$  lies at a value anomalously low compared with the energy scale of the SLAFM, as deduced from QMC [34] and HTSE methods [35, 36]; again this result reflects directly the effects of frustration in suppressing the overall energy scale of the magnetic excitations [26].

The magnetic entropy,  $S_m(T) = \int C_m/T dT$ , which we calculate from our  $C_m(T)$  data by integrating above 0.08 K, is shown in Fig. 1(f). At 7.5 K, we estimate that  $S_m(T)$  saturates  $90 \pm 10\%$  of its total value,  $S_m(\infty) = R \ln 2$  for a spin-1/2 system. If the system were to order at the lowest temperatures ( $T < 0.08$  K), one might

expect some of the entropy to remain unaccounted for. However, because of the errors accumulated in the integration, including those from the phonon subtraction, we cannot draw any meaningful conclusions about possible missing entropy from this result, other than that it is small. If, on the other hand, the ground state were to have a spin gap, again our entropy results are consistent with a value below 0.05 K [Fig. 1(f)].

What we find at our lowest temperatures is that  $S_m(T)$  has a very rapid initial increase from  $T = 0.08$  K, with 33% of  $S_m(\infty)$  recovered by  $T = 0.3$  J [inset, Fig. 1(f)]. Here we compare our data to the reconstructed Schwinger-boson mean-field (RSBMF) approach [23], a modified Schwinger-boson technique that accounts correctly for the number of physical spin states and thus is designed to capture the key properties of the TLAFM in the low-temperature regime. By comparison with our data, the RSBMF formalism provides semi-quantitative accuracy over the temperature range illustrated (which matches the authors' claim for the validity of the method). However, the form of  $S_m(T)$  at lower temperatures is not well described, a result on which we comment briefly below. Nevertheless, we note for perspective that the type of nonlinear- $\sigma$ -model approach so effective for the SLAFM recovers only 5% of the total entropy at  $T = 0.3$  J in the TLAFM [25, 37] and therefore appears incapable of providing a suitable account of frustrated systems.

We conclude that, over the full range of temperatures covered by our thermodynamic measurements,  $\text{Ba}_8\text{CoNb}_6\text{O}_{24}$  behaves as a model 2D  $S = 1/2$  TLAFM. Concerning the Hamiltonian governing the behavior of the effective  $S = 1/2$  spins, by comparison with the analysis of Ref. [28], our  $\chi_s(T)$  and  $C_m(T)$  data contain no evidence for an XXZ anisotropy, of Ising or XY type. Thus within the error bars of our thermodynamic measurements, the effective model realized by the material is a Heisenberg TLAFM. At a more microscopic level, an effective Heisenberg interaction implies that the trigonal distortion of the  $\text{CoO}_6$  octahedra, denoted by  $\delta$  in Refs. [14, 31], should vanish. In the structural refinement performed on the basis of our powder x-ray diffraction measurements, we indeed obtain an excellent account of our data without any trigonal distortion, and thus find no evidence for a finite  $\delta$  parameter within the error bars of the fitting process.

## IV. NQR and NMR Measurements

### A. NQR and candidate QSL

To probe both static and low-energy magnetic properties, we begin at zero field by presenting low-temperature  $^{93}\text{Nb}$  NQR data. Here we report only the signal with the shortest spin-lattice relaxation time,  $^{93}\text{T}_1$ , which is over three orders of magnitude lower than the other times present and arises in all probability from the Nb sites

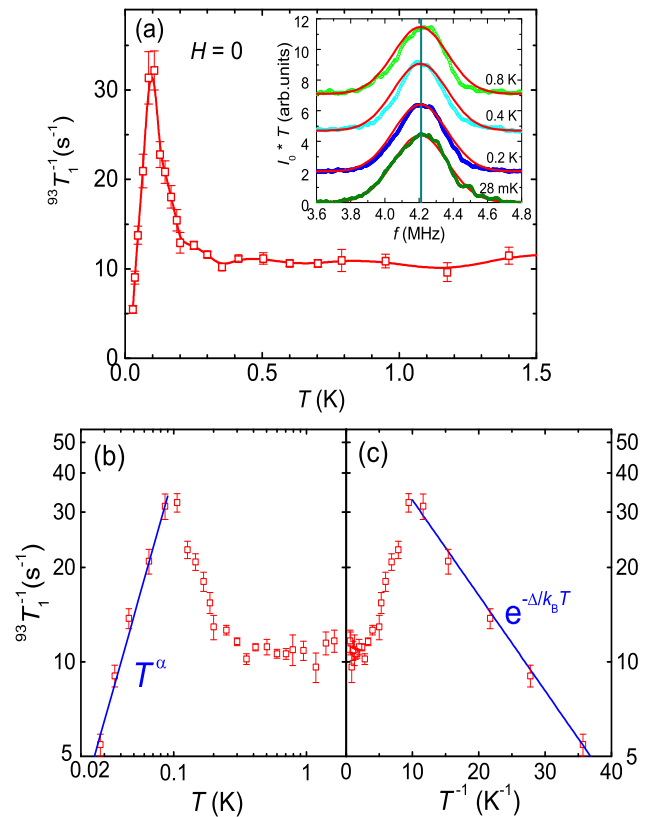


FIG. 2. **NQR measurements on  $\text{Ba}_8\text{CoNb}_6\text{O}_{24}$ .** (a) Spin-lattice relaxation rate,  $1/^{93}\text{T}_1$ , measured at zero field as a function of temperature. The upturn below 0.2 K indicates a progressive increase of the correlation length upon cooling, which is cut off abruptly below 0.1 K. Inset: zero-field  $^{93}\text{Nb}$  NQR spectra for temperatures from 0.8 K to 0.028 K, with the measured intensity multiplied by  $T$ . Red lines represent the Gaussian fit to the spectrum at 0.028 K overlaid on all four datasets. (b)  $1/^{93}\text{T}_1$  data on logarithmic axes. The straight-line fit (blue) indicates an approximate power-law form,  $1/^{93}\text{T}_1 \propto T^\alpha$  with  $\alpha = 1.51 \pm 0.06$ . (c)  $1/^{93}\text{T}_1$  data on semi-log axes as a function of inverse temperature. The straight-line fit (blue) indicates an approximate activated form with energy gap  $\Delta = 0.070 \pm 0.003$  K.

closest to the  $\text{Co}^{2+}$  layers (i.e. with strong hyperfine coupling to the  $\text{Co}^{2+}$  moments). The  $^{93}\text{Nb}$  NQR spectra for excitations between  $I_z = \pm 9/2$  and  $I_z = \pm 7/2$  are shown in the inset of Fig. 2(a) for temperatures from 0.8 K down to 0.028 K and with their intensity,  $I_0$ , corrected for the Zeeman factor,  $1/T$ . At  $T = 0.028$  K, the spectrum is well fitted by a Gaussian function (red line), and this fit can be applied also to the spectra at 0.2 K, 0.4 K, and 0.8 K. Clearly the spectra at all temperatures are centered on one maximum, at the resonance frequency  $f = 4.212$  MHz ( $4\nu_q$ ), and all have the same echo intensity. The absence of any signal loss or NQR frequency shift excludes completely the onset of any magnetic order down to 0.028 K. Because the  $^{93}\text{Nb}$  nucleus is located directly above the center of one triangle composed of three  $\text{Co}^{2+}$  ions [Fig. 1(b)], the static hyperfine field at each  $^{93}\text{Nb}$  site

should, if the  $\text{Co}^{2+}$  moments order with the  $120^\circ$  coplanar pattern [10], have an appreciable component normal to the TLA FM plane. Thus it is highly unlikely that magnetic order could be missed in the NQR spectra.

The NQR spin-lattice relaxation rate shown in Fig. 2(a) probes the low-energy spin fluctuations. In general,  $1/T_1 T = \sum_q A_{\text{hf}}(q) \text{Im}\chi^\pm(q, \omega)/\omega|_{\omega \rightarrow 0}$ , where  $A_{\text{hf}}$  is the hyperfine coupling constant and  $\chi^\pm(q, \omega)$  the transverse dynamic susceptibility. The fact that  $1/^{93}\text{T}_1$  is of order  $10 \text{ s}^{-1}$  indicates rather strong hyperfine coupling between the  $^{93}\text{Nb}$  nucleus and the  $\text{Co}^{2+}$  spins.  $1/^{93}\text{T}_1$  also contains no evidence for long-range order, but its upturn below 0.2 K indicates an increasing correlation length, precisely as would be expected if the system approaches the zero-temperature magnetic order anticipated by the Mermin-Wagner theorem [11]. To our knowledge, such a direct observation of incipient “Mermin-Wagner order” in a purely 2D magnetic system has not hitherto been obtained.

However, this textbook-quality Mermin-Wagner divergence is cut off quite abruptly at 0.1 K, as Fig. 2(a) shows clearly. Instead of continuing to diverge as the temperature decreases, the  $1/^{93}\text{T}_1$  signal shows a sharp peak and a rapid drop to very low values. We stress again that the temperature-normalized spectra are almost identical for all temperatures [inset, Fig. 2(a)], and that all of the magnetization recovery curves we measure contain no sign of a stretched exponential form. As noted above, these results provide no evidence for splitting or broadening of the peak, as would occur in a finite- $T$  ordered phase. Similarly, they contain no evidence for any spin-freezing, or other types of spin-glass behavior, at such a low temperature, ruling out an inhomogeneous origin for the drop in  $1/^{93}\text{T}_1$ . Despite the normalized echo intensities remaining constant for all temperatures, a weak signal loss is observed close to 100 mK, which reinforces the evidence for very strong low-energy spin fluctuations coinciding with the peak in  $1/^{93}\text{T}_1$ . Thus these features appear to be clear evidence for a transition or abrupt crossover to a zero-temperature magnetically disordered phase, which is a candidate for an intrinsic QSL.

At the experimental level, a QSL is typically analyzed by considering the temperature dependence of the spin-lattice relaxation rate. An algebraic form indicates a gapless QSL while an exponential (activated) form indicates a gapped QSL. Figure 2(b) shows the data of Fig. 2(a) on logarithmic axes, which suggest a functional form  $1/^{93}\text{T}_1 \propto T^\alpha$ , i.e. a gapless QSL with  $\alpha = 1.51 \pm 0.06$ . By contrast, Fig. 2(c) shows the same data in the activated form, which returns at least as good a fit to a gapped QSL with  $\Delta = 0.070 \pm 0.003 \text{ K}$ . We comment that the quoted errors are only statistical, and do not include systematic errors. The only conclusion one may draw is that it is impossible to make any meaningful deductions from a fit to five data points covering half a decade in temperature. However, the very low temperature scales involved make it impossible to broaden the fitting window. Under the gapless scenario, such a small and half-integer exponent

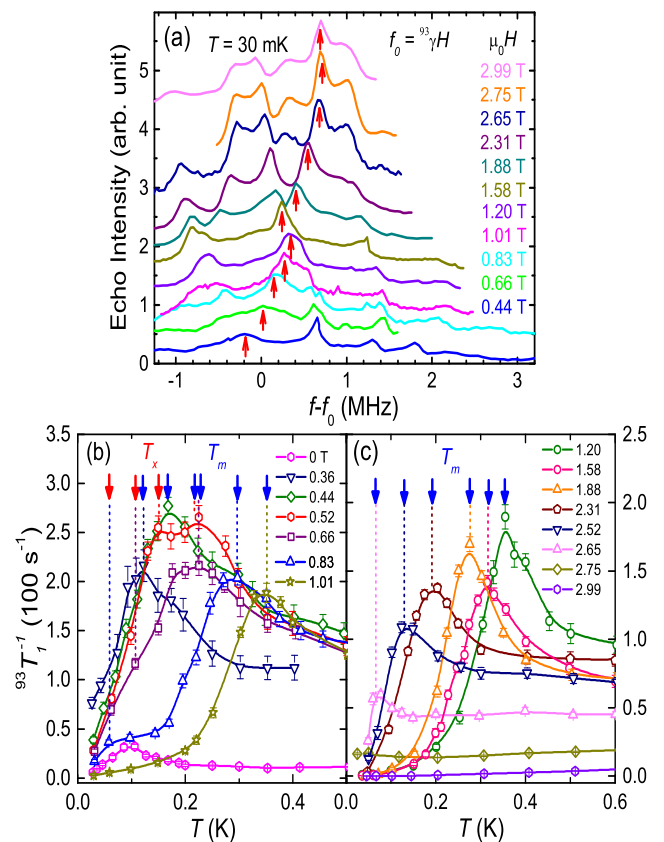


FIG. 3. **NMR response of  $\text{Ba}_3\text{CoNb}_6\text{O}_{24}$  over a range of applied fields.** (a)  $^{93}\text{Nb}$  field-sweep spectra displayed as a function of frequency,  $f - f_0$ , at a fixed temperature  $T = 30 \text{ mK}$ . The reference frequency  $f_0 = ^{93}\gamma H$  is defined for each spectrum from the measurement field,  $H$ , given in the legend. The spectra are offset vertically for clarity. Arrows mark the spectral peak where the spin-lattice relaxation rate,  $1/^{93}\text{T}_1$ , is measured. (b)  $1/^{93}\text{T}_1$  shown as a function of temperature for selected low fields. (c)  $1/^{93}\text{T}_1(T)$  for selected high fields. Blue arrows mark the positions of the peaks we take to indicate the magnetic transition. Red arrows for certain field values in panel (b) mark a lower characteristic feature (see text).

would have to be the consequence of spin fractionalization. Under the gapped scenario, such a small gap (of order  $J/25$ ) would have few consequences at all conventional experimental temperatures (and is very difficult to probe). The only unambiguous conclusion from our NQR results is that new physics sets in at an interaction energy scale of order 0.1 K. We defer a discussion of possible theoretical scenarios to Sec. V.

## B. NMR and $(H, T)$ Phase Diagram

To investigate the situation in more detail, we expand our studies of the TLA FM to finite magnetic fields by performing NMR measurements at applied fields up to and beyond saturation. Figure 3(a) shows  $^{93}\text{Nb}$  NMR

spectra taken over the full range of field values, all of which have a dominant feature centered close to the frequency  $f_0 = {}^{93}\gamma H$ , where  ${}^{93}\gamma = 10.421$  MHz/T is the gyromagnetic ratio of  ${}^{93}\text{Nb}$ , accompanied by a number of other features spanning a broad frequency range. We stress that the entire spectrum is the contribution of one single type of  ${}^{93}\text{Nb}$  site, due to the  $I = 9/2$  nuclear spin and the powder sample, as we discuss next.

For the powder sample we have available, the NMR spectra show very strong broadening due to the combination of quadrupolar corrections [38], anisotropic field effects, and the anisotropy of the hyperfine coupling in the TLAFM [39]. While this makes a full assignment of the different resonance frequencies to different field-orientation distributions an impossible task, we begin our interpretation of the NMR data at high fields,  $H > H_s$ . The spectrum at 2.99 T has a peak around  $f - f_0 = 0.7$  MHz, whose position [marked by the arrows in Fig. 3(a)] changes more rapidly with decreasing field than any other feature. This indicates a strong hyperfine field with one specific orientation. Although it is not possible to verify, this peak is consistent with an NMR center line for field orientation  $H\parallel ab$  for three reasons: i) it is close to  $f - f_0 = 0$ ; ii) for layered compounds,  $H\parallel ab$  is the most probable orientation in a powder sample; iii) the hyperfine coupling is highly anisotropic from  $H\parallel ab$  to  $H\parallel c$ , as observed for the Ba(2) sites in  $\text{Ba}_3\text{CoSb}_2\text{O}_9$  [39], which ensures a significant separation of contributions due to different crystallite orientations. On this basis, the broad feature with frequencies from 0.2 to 1.2 MHz at 2.99 T can be ascribed to the combination of a distribution of hyperfine fields (which vary linearly with the Larmor frequency,  $\nu_L$ ) and a distribution of second-order quadrupolar corrections (which vary as  $\nu_q^2/\nu_L$  [38]), both due to crystallites with orientations close to  $H\parallel ab$ . By contrast, the broad peak from  $-0.4$  to 0 MHz may be associated with field orientations close to  $H \parallel c$ , where the hyperfine fields are weaker [39]; however, these assumptions should be verified by single-crystal NMR studies when possible. Finally, the resonances visible in the spectra at  $|f - f_0| \geq 1$  MHz are due to satellite transitions, which in an  $I = 9/2$  system are shifted from the center line by  $\pm\nu_q$ ,  $\pm 2\nu_q$ ,  $\pm 3\nu_q$ , and  $\pm 4\nu_q$  [38].

To compare the spectra in a consistent manner, we focus only on the prominent center peak of each one, which is marked by the arrows in Fig. 3(a). As the applied field is increased, the peak position shifts to a higher frequency, which indicates an increase of the local hyperfine field. However, although the shift  $f - f_0$  is caused primarily by the hyperfine-field contribution at applied fields above 1 T, it is contaminated strongly by the quadrupolar corrections at low fields [38].

Here we make two comments of relevance to the discussion below. First, an integral feature of the finite-field phase diagram of the TLAFM is the “up-up-down” state, of two field-aligned and one anti-aligned spin(s) per triangle. Our estimate of the line shift resulting from an up-up-down phase of field-induced order in  $\text{Ba}_8\text{CoNb}_6\text{O}_{24}$  is

approximately 230 kHz. This value is 1/3 of the shift observed in the fully polarized state ( $H > H_s$ ) and is the same at all Nb sites, with the result that there is no splitting. However, the presence of such a shift is not well established in our data, due not least to the growing quadrupolar corrections at lower fields. Second, our NMR spectra contain no evidence for the mixing of Co and Nb sites, i.e. for an extrinsic source of disorder. While one may postulate that nonmagnetic Nb impurities in the Co TLAFM, and magnetic off-plane Co impurities, may have a significant effect on the properties of  $\text{Ba}_8\text{CoNb}_6\text{O}_{24}$ , we are unable to identify any inequivalent Nb sites. In the closely related material  $\text{Ba}_3\text{CoNb}_2\text{O}_9$ , two very sharp magnetic ordering transitions are observed [17], which serves again to underline how weak such disorder effects appear to be in the Co-Nb system. Further, the magnetization recovery  $[I(t)]$  we measure at all fields and temperatures fits very well to the standard function (Sec. II), which again reinforces the message of excellent sample quality.

In Figs. 3(b) and 3(c) we show as functions of temperature the NMR spin-lattice relaxation rates, also denoted  $1/{}^{93}T_1$ , measured at the frequency of the spectral peak. A sharp maximum is clearly visible at every applied field. The general trend is that the peak value of  $1/{}^{93}T_1$  increases strongly with field up to  $\mu_0 H \approx 0.5$  T, before decreasing more slowly up to fields beyond  $H_s$ . We have verified (data not shown) that such a relaxation peak is also present when measured at different frequencies in all spectra, which indicates very strongly that this form of behavior is intrinsic. The temperature at which the peak appears, marked by the arrows in Figs. 3(b) and 3(c), varies systematically with the field, increasing to  $T_m \approx 0.35$  K at  $\mu_0 H = 1.20$  T before falling monotonically to zero at  $H = H_s$ .

A pure Heisenberg model in an applied magnetic field retains a rotational symmetry about the field axis. However, the  $\text{Ba}_8\text{CoNb}_6\text{O}_{24}$  system has crystalline anisotropies and spin-orbit coupling in addition to possible experimental misalignments, as a result of which it is realistic to take the field as an explicit breaking of the continuous spin symmetry. In this event, the Mermin-Wagner theorem is no longer applicable and a real magnetic order is induced, even in 2D, until it is suppressed by thermal fluctuations. Thus we ascribe the peak in the NMR  $1/{}^{93}T_1$  to a real magnetic ordering transition occurring at temperature  $T_m$ , below which the ordered phases have an anisotropy gap. The magnetic transition in  $\text{Ba}_3\text{CoSb}_2\text{O}_9$  was also reported on the basis of the peak in  $1/T_1$  [39], although in this material the order sets in at 3.8 K at zero field due to interlayer (3D) coupling. At  $H = 0.52$  T, we find a curious double-peak structure, which by the same reasoning should be associated with a second characteristic temperature scale. At  $H = 0.88$  T, the lower temperature appears not as a peak but as a second sharp drop, occurring around  $T = 0.06$  K at the lower end of a plateau in the relaxation rate. As one of these forms evolves into the other, our ascription of a

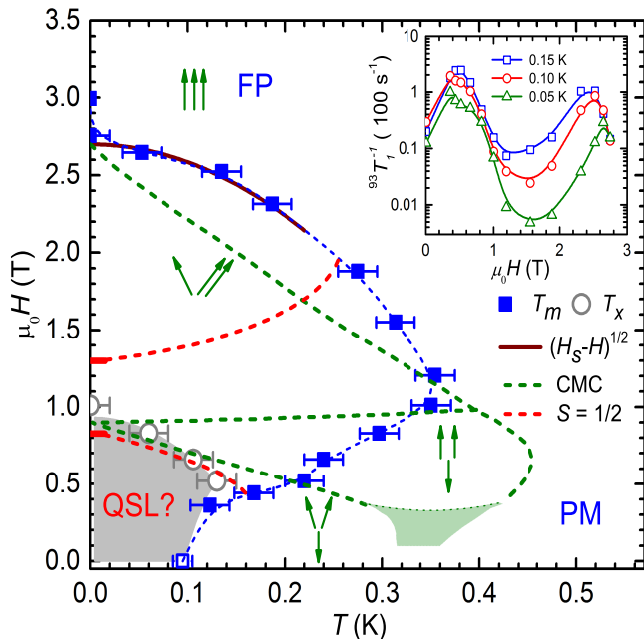


FIG. 4. **Field-temperature phase diagram of  $\text{Ba}_8\text{CoNb}_6\text{O}_{24}$ .**  $(H, T)$  phase diagram constructed from the spin-lattice relaxation rate. Solid blue squares represent the temperature of the peak in  $1/^{93}T_1$ , taken from Figs. 3(b) and 3(c), and open grey circles mark the lower temperature scale found in  $1/^{93}T_1$  at low fields [Fig. 3(b)] (see text). The shaded region demarcates the candidate quantum spin liquid phase. The solid line is a fit of the upper transition to the functional form  $T_c(H) = c(H_s - H)^{0.5}$ . Green arrow symbols and dashed lines represent the phases and phase boundaries established by Monte Carlo simulations of the classical TLAFM, adapted from Refs. [40] and [41] and scaled to  $J = 1.66$  K. Red ticks on the field axis at  $T = 0$  mark the boundaries of the up-up-down phase for the  $S = 1/2$  Heisenberg TLAFM, established by many authors and taken in this case from Ref. [42]. Red dashed lines mark schematic finite-temperature phase boundaries anticipated for the up-up-down phase in the  $S = 1/2$  system, where it is favored by quantum fluctuations. Inset: field dependence of  $1/^{93}T_1$  shown at fixed temperatures of 50, 100, and 150 mK. The presence of only two peaks suggests that the entire intermediate regime accessible in experiment may have only one type of field-induced order.

second temperature scale,  $T_x$ , to a weak feature in the  $\mu_0 H = 0.66$  T data is very tentative. At 1.01 T, the feature and hence  $T_x$  has clearly vanished.

In Fig. 4, we gather the  $T_m$  and  $T_x$  values determined from  $1/^{93}T_1$  in the form of an  $(H, T)$  phase diagram.  $T_m$  demarcates a regime of field-induced magnetic order below  $H_s \simeq 2.7$  T and a maximum temperature of 0.35 K, while  $T_x$  may be the upper limit in field of the anomalous disordered region we find by NQR (Fig. 2, marked by the shaded region in Fig. 4). As a guide to interpreting our results, we have annotated Fig. 4 with a number of other lines. Green dashed lines show the phase boundaries obtained by Monte Carlo studies of classical (large- $S$ ) Heisenberg TLAFM [40, 41], which obtain the four

finite- $H$  phases represented by the green arrows, namely distorted triangular, up-up-down, canted, and fully polarized. The red bars on the field axis ( $T = 0$ ) represent the boundaries of the up-up-down plateau of the fully quantum  $S = 1/2$  Heisenberg TLAFM, obtained by a number of methods and taken here from Ref. [42]. We stress two features of the  $S = 1/2$  results, first that the same four phases obtained in the classical model are present in the quantum case and second that, in contrast to the classical case, the up-up-down plateau has a finite width at  $T = 0$  as a result of its stabilization by quantum fluctuations, which have a generic preference for antiparallel spin configurations. Based on this expectation, the red dashed lines sketch the possible phase boundaries of the quantum up-up-down plateau at finite  $T$ . We stress that these lines rank as no more than guides to the eye. There is as yet no theoretical or numerical method that is capable of drawing the  $(H, T)$  phase diagram of the  $S = 1/2$  TLAFM, which is a major reason why experimental results for an almost-perfect TLAFM material such as  $\text{Ba}_8\text{CoNb}_6\text{O}_{24}$  are so important. The downward curvature of the lower boundary and upward curvature of the upper one are based on the expectation that thermal fluctuations will favor the collinear-spin up-up-down phase over the non-collinear distorted triangular and canted phases (but the extent of this curvature is in essence unknown). A very recent experiment has investigated the spin excitations of the up-up-down state in  $\text{Ba}_3\text{CoSb}_2\text{O}_9$  [43], i.e. in the presence of finite 3D coupling and easy-plane anisotropy.

Because our measurements are performed on powder samples, it is very difficult to determine the magnetic structure. In particular, the difference between collinear and non-collinear ordered phases becomes even more difficult to discern. In the inset of Fig. 4 is shown  $1/^{93}T_1$  as a function of field at the fixed temperatures  $T = 50, 100,$  and  $150$  mK. By the same criterion as in Figs. 3(b) and 3(c), these curves suggest that there are only two significant phase transitions as the field is increased, and thus that the entire magnetically ordered phase may be of only one type, rather than the anticipated three. We stress for clarity that, despite the presence of the anomalous candidate QSL regime at low  $T$  and  $H$  (shaded in Fig. 4), one would still expect to recover the behavior of the conventional  $S = 1/2$  TLAFM for  $T > 0.1$  K (where thermal fluctuations overwhelm the additional low energy scale) and for  $H > 1$  T (where, empirically, the field suppresses quantum fluctuations to a sufficient degree).

The possible origin of the candidate QSL is discussed in Sec. VC. Outside this regime, we can use our experimental measurements on  $\text{Ba}_8\text{CoNb}_6\text{O}_{24}$  to benchmark the quantum phase diagram of the spin-1/2, 2D Heisenberg TLAFM in a manner that has not been possible before. We identify four ways in which quantum fluctuations act to revise the classical phase diagram. (i) The field,  $H_{\text{max}}$ , at which the maximum value of  $T_m$  occurs is 80% higher in the  $S = 1/2$  system than in the classical case. (ii) In the classical Monte Carlo simulations, there



are one or possibly two finite-temperature phase transitions at very weak fields, but in the  $S = 1/2$  system this regime is entirely paramagnetic and the lower bound on the ordered regime has a finite slope. (iii) In the classical model, the phase boundary to the fully polarized state approaches  $H_s$  linearly, whereas in the  $S = 1/2$  system the phase boundary is fitted rather well, over approximately one decade of data in temperature, by the form  $T_m(H) \propto (H_s - H)^{1/2}$ . (iv) In the classical model one expects three different ordered phases under the dome of  $T_m(H)$ , whereas in the experimental measurements there is no evidence for a change of phase at finite temperatures. We discuss these four points in detail in Sec. VB.

## V. Discussion

### A. Zero-field quantum physics: Mermin-Wagner

The physics of a 2D quantum magnet with continuous symmetry is controlled by the Mermin-Wagner theorem. While thermal fluctuations can act to reinforce quantum fluctuations in gapped systems, their effect on candidate ordered phases is a systematic suppression. Thus in experiment one may observe only an incipient order, which is best characterized by a correlation length,  $\xi$ , or time,  $\tau$ , that increases with decreasing temperature towards a divergence at  $T = 0$ . This is exactly the behavior we observe in the NQR spin-lattice relaxation rate, shown in Fig. 2(a), where the diverging trend becomes clear below 0.2 K. However, the presence of the anomalous disordered state at the lowest temperatures ( $T < 0.1$  K) spoils a more systematic characterization of this divergence.

The TLAFM is a keystone model in quantum magnetism because it offers one of the basic realizations of a geometry that is frustrated for AFM interactions. At zero field, where one may wish to investigate the consequences of frustration for thermodynamic quantities, correlation functions, and the dynamical response, its primary effect is the suppression of characteristic energy scales. For a deeper understanding of the anomalous low energy scale observed in the thermodynamic quantities of Fig. 1, the most sophisticated methods available for the Heisenberg TLAFM are HTSE [19, 26], self-consistent spin-wave [20, 21], and RSBMF treatments [23]. These indicate that the one-triplet excitation band is both extremely flat and unusually low-lying, with most of its weight concentrated around  $E \approx 0.6J$ , similar to the recent observation in  $\text{Ba}_3\text{CoSb}_2\text{O}_9$  [24]. This is a direct consequence of the band being driven downward by the low-lying two-triplet excitation continuum, which shows strong triplet interactions at all wave vectors due to the high frustration. This behavior stands in sharp contrast to the SLAFM, where the bands disperse uniformly up to energies  $E \approx 2J$  [44]. The frustration-renormalized energy scale is completely consistent with the temperature dependence we benchmark in the peak features of  $\chi(T)$  and  $C_m(T)$ . The unusual low-energy excitations of the

TLAFM have been variously described as “roton-like” or as evidence of fermion deconfinement [19, 20].

To our knowledge,  $\text{Ba}_8\text{CoNb}_6\text{O}_{24}$  allows the first direct comparison between theory and a real 2D material for the  $S = 1/2$  Heisenberg TLAFM. If one takes seriously the small but finite quantitative discrepancies between the HTSE results [25] and our data for  $C_m(T)$  [Fig. 1(e)] and  $\chi(T)$  [Fig. 1(d)], one requires an explanation for possible additional contributions on the low side of the peaks in both quantities. The specific heat contains contributions from all types of excitation, and appears to show unexpected weight around 0.5 K. The susceptibility is sensitive only to finite-spin excitations, primarily triplets ( $S = 1$ ), and the peak in this quantity appears to lie at a temperature 10-15% lower than HTSE would forecast. Thus it is possible that this method is not quite capturing the full extent of the suppression of the one-triplet band due to the frustration of the TLAFM. Experimental uncertainties notwithstanding, the RSBMF approach appears to underestimate the low-temperature entropy [Fig. 1(f)] and may not be capturing the correct temperature dependence. One possible exotic explanation for this result [45] might be the incomplete binding of spinon degrees of freedom contained within the slave bosons.

More generally, both results may be explained if the “roton gap,” the effective bandwidth, the weight in the two-triplet sector, or any other features affecting the density of states in the spin spectrum, all of which require a correct accounting for quantum fluctuation effects, are not reproduced perfectly by the theoretical or numerical approaches applied. However, we caution that the small mismatch between our data and the theoretical results shown in Fig. 1 cannot be interpreted unambiguously as evidence for shortcomings in the theories, as it may be a consequence of experimental uncertainties, particularly in the entropy, or of small additional terms in the magnetic Hamiltonian. While it is clear from the appearance of the candidate QSL phase (Sec. VC) that such terms are indeed present, we comment that energy scale for the QSL regime does not match the temperatures at which the discrepancies in  $\chi(T)$  and  $C_m(T)$  appear, although it could indeed be relevant for the interpretation of  $S_m(T)$ . A notable candidate for such a term would be a weakly non-Heisenberg anisotropy in the exchange couplings, which is already documented in  $\text{Ba}_3\text{CoNb}_2\text{O}_9$ , although we are unable to obtain any evidence for this in our measurements. We defer a further analysis of this point until single crystals become available.

### B. Quantum fluctuation corrections

Here we discuss the differences between the classical and measured (“quantum”) phase diagrams shown in Fig. 4, retaining the numbering scheme of Sec. IVB.

(i) The field at which the maximum of  $T_m$  appears in the classical case,  $H_{\text{max}} \approx 2J$  in dimensionless units, coincides with the center of the most stable of the ordered

phases, which is the up-up-down phase. The very significant (approximately 80%) rise of this optimum field in the quantum system appears to reflect the much greater stability of the up-up-down phase due to the strong quantum fluctuations of the  $S = 1/2$  system. In fact our choice of the position of the upper red dashed line in Fig. 4 was made on the basis of an approximate symmetry criterion with respect to  $H_{\max}$ .

(ii) In the classical Monte Carlo simulations, there is a problem at zero field in that order is precluded by the Mermin-Wagner theorem but is present at a finite temperature at any finite field. In the quantum case, the lower bound on the ordered regime has a finite slope, which has a clear interpretation in terms of the competition between the disordering effects of thermal fluctuations and the ordering effects of a rising field. The slope of this line, which is approximately linear if the QSL regime is ignored, would be one topic for a more detailed analysis. We comment that the shaded region in the classical Monte Carlo phase diagram denotes an uncertainty over the nature of the thermal transition(s) that is reflected in a contrast between the results of Refs. [40] and [41], but that this appears to be a moot point in the quantum system.

(iii) The contrasting functional forms of the magnetic phase boundary near saturation,  $T_m(H) \propto (H_s - H)^a$  with  $a = 1$  in the classical system and  $a = 0.5$  in the quantum one, can be taken as a direct expression of the qualitative differences resulting from quantum fluctuations. In this case their effect is to confer extra stability on the field-induced ordered phase, possibly changing its nature [point (iv) below], and to alter the way in which this order is lost as thermal fluctuations increase.

(iv) More mysterious is the nature of the field-induced ordered phase. As noted in Sec. IVB, three different ordered phases are expected between  $H = 0$  and  $H = H_s$  in the classical model, and in the quantum model at  $T = 0$ . Our experiments offer no evidence for a change of phase. Taking this result at face value, it is possible that the thermal destabilization of the non-collinear phases (distorted triangular and canted) in favor of the collinear up-up-down phase is truly a strong effect, which is complete below 50 mK in  $\text{Ba}_8\text{CoNb}_6\text{O}_{24}$ . However, as also discussed above, it is difficult to exclude the possibility that the three ordered phases are simply indistinguishable in the present powder experiments.

### C. Quantum disordered phase

The most surprising feature of our results is the appearance of the magnetically disordered phase at low temperature and low fields. Such a phase is not expected in any studies of the  $S = 1/2$  TLAFM at zero field or zero temperature. Clearly the most basic question to address is whether this phase is a consequence of intrinsic quantum physics, due to a weak additional term in the magnetic Hamiltonian, or whether it could arise from an

extrinsic factor, such as sample disorder. While it is difficult to make a definitive statement about this eventuality, the most obvious type of randomness in  $\text{Ba}_8\text{CoNb}_6\text{O}_{24}$  would be “anti-site” disorder, namely non-magnetic Nb ions in the Co planes and magnetic Co ions on some of the Nb sites. Nonmagnetic sites (vacancies) in an ordered 2D  $S = 1/2$  magnet are found in theoretical studies [46] to cause a weak reinforcement of order, at least if virtual electronic hopping to the site is also prohibited. In the  $\text{Ba}_8\text{CoNb}_6\text{O}_{24}$  geometry, a Co ion off the plane might be expected to form a net singlet state with the three spins of the neighboring in-plane triangle, creating an effective three-site vacancy, and for the same reason this should not lead to a magnetically disordered phase. In experiment, all types of disorder have rather clear fingerprints in the NMR spectra, and as noted in Sec. IVB we are not able to detect any spectral features corresponding to Nb ions with a different type of environment.

Another extrinsic factor would be the coupling of the electronic spins to the nuclear-spin subsystem. In ordered magnetic materials, this coupling can give rise to a shift, or “pulling” [47], of the NMR frequency and a significant literature has built up concerning the measurement and quantitative description of this effect, particularly in Mn-ion systems [48]. To estimate whether the interaction with nuclear spins could be responsible for our observations, we first consider the magnitude of the hyperfine coupling. The transferred hyperfine coupling from the Co electronic spins to the Nb nuclear spins, which is the pathway by which we probe the TLAFM in  $\text{Ba}_8\text{CoNb}_6\text{O}_{24}$ , has an interaction constant  $A_{\text{hf}} = 0.04$  T per  $\mu_B$ . The associated energy scale is calculated as  $E_{\text{hf}} = \gamma A_{\text{hf}} I S$ , where  $S = 1.9\mu_B$  is the magnetic moment per Co electronic spin and  $I = 9/2$  the Nb nuclear spin, whence  $E_{\text{hf}} = 0.14$  mK, which is much too small to be relevant to our observations. However, there is also a direct hyperfine coupling of the Co electronic to the Co nuclear spins ( $I = 7/2$ ), which is approximately  $A'_{\text{hf}} = 5$  T per  $\mu_B$  in systems with local Co-ion coordination similar to that in  $\text{Ba}_8\text{CoNb}_6\text{O}_{24}$  [49], and the resulting energy scale can be estimated as  $E'_{\text{hf}} = 0.016$  K. Once again, this channel appears too small to be responsible for effects setting in at 0.1 K, as we observe in Figs. 2, 3, and 4.

Qualitatively, it is in any case not clear how the hyperfine interaction would affect the electronic spin state in a thermally disordered magnetic phase, of the type relevant here down to 0.1 K. Pulling requires a finite ordered moment to produce the observed frequency shift [50]. In the Ising magnet  $\text{LiHoF}_4$  [51], coupling to the nuclear spins acts to extend the regime of magnetic order of the electronic spin system, which is the opposite of the physics we observe. On general grounds, a coupling of the electronic spin system to the very high density of low-energy excitations introduced by the nuclear-spin system does not seem likely to establish a situation where the density of low-energy spin excitations appears to vanish towards zero energy. In one study of nuclear-

spin coupling to a disordered electronic spin system [52], the magnetic spectrum of the composite system remains gapless for systems with no nontrivial topological term, which should be the relevant one in 2D, and does not appear to lose low-energy weight. Although the coupled Hamiltonian belongs to the general class of Kondo-type models, it is difficult to conceive of Kondo-type physics (local singlet formation) for localized electrons interacting with  $I = 7/2$  nuclear spins. Thus, within the scope of the present study, we conclude that nuclear-spin coupling cannot present a candidate origin for our observations. We recall that, in an intrinsic state of the electronic spins alone, the mutual interaction energy scale ( $J = 1.66$  K) is two orders of magnitude higher than the hyperfine coupling scale.

Turning to a possible intrinsic origin, we begin by reviewing other candidate terms in the magnetic Hamiltonian. A 3D coupling is not expected on an energy scale of 0.1 K in a system as 2D as  $\text{Ba}_8\text{CoNb}_6\text{O}_{24}$ , and in any case this would promote finite-temperature order. Motivated by the material  $\text{Cs}_2\text{CuCl}_4$  [12], which shows QSL behavior in a spatially anisotropic TLAFM, systems in which every triangle has one strong and two weak bonds have been of enduring interest [53]. However, there is no evidence in the NMR spectra for the onset of a low-temperature lattice distortion, which would also be most unexpected at such low energy scales.

Spin-orbit coupling has been studied intensively in insulating magnets as the possible origin of chiral QSL states and Kitaev spin liquids. In conventional local-moment systems, spin-orbit coupling is manifest in the Dzyaloshinskii-Moriya interaction on chemical bonds lacking inversion symmetry and in exchange anisotropies on inversion-symmetric bonds. For the  $\text{Co}^{2+}$  ions in  $\text{Ba}_8\text{CoNb}_6\text{O}_{24}$ , the spin-orbit energy scale,  $\lambda \approx 250$  K, is strong and the lowest Kramers doublet of the crystal-field manifold defines the effective  $S = 1/2$  degree of freedom, along with a possible exchange anisotropy in the event of a finite trigonal distortion [14, 31]. Within this effective model, the possibility of effective Dzyaloshinskii-Moriya interactions is excluded by the fact that the bonds of the  $\text{Ba}_8\text{CoNb}_6\text{O}_{24}$  lattice [Figs. 1(a) and 1(b)] are inversion-symmetric (unless sample disorder were to produce such terms around an impurity). Although an effective exchange anisotropy is the strongest candidate for an additional term in the spin Hamiltonian, we stress that XXZ physics has been found to produce no abrupt or significant changes to the zero-temperature phase diagram [54], and thus that such a term would not be capable of creating a disordered magnetic state. Indeed, the fact that this term breaks the continuous symmetry, in whole or in part, thereby lifting the Mermin-Wagner constraint, would seem more likely to promote magnetic order than to suppress it. While anisotropy of the single-ion type is not relevant for  $S = 1/2$  systems, the situation for the effective  $S = 1/2$  entities in  $\text{Co}^{2+}$  is more complex. In this context it is worth noting that a temperature-driven effective-low-spin to high-spin crossover appears to oc-

cur in  $\text{Ba}_3\text{CoNb}_2\text{O}_9$  between 100 and 200 K [17], i.e. on the energy scale of  $\lambda$ , but it remains difficult to invoke such behavior (which is governed by  $d$ -level crystal-field splittings on 100 meV energy scales) at 0.1 K.

Of the limited selection of remaining candidate mechanisms, a next-neighbor coupling,  $J_2$ , has been shown [55–58] to produce a QSL in the narrow range of interaction strengths  $0.06 \lesssim J_2/J \lesssim 0.17$ . While all of the recent studies agree rather closely on the boundaries of this regime, they are completely divided on the nature of the QSL, with variational Monte Carlo (VMC) methods suggesting a gapless state [56], also supported by the use of more sophisticated quantum-number projection [59] and ground-state refinement methods [60], DMRG suggesting a gapped one [58, 61], and the coupled-cluster method being unable to comment [57]. Because studies of the QSL ground state of the kagome lattice indicate that VMC has a generic preference for gapless phases and DMRG for gapped ones, there is little to learn from these results. The problem with this interpretation in  $\text{Ba}_8\text{CoNb}_6\text{O}_{24}$  is that a  $J_2$  interaction requires a Co-O-(Nb)-O-O-(Nb)-O-Co path, whose shortest realization passes through one  $\text{NbO}_6$  octahedron below the plane and one above it, via another in-plane  $\text{CoO}_6$  octahedron [Fig. 1(b)]. An alternative path with both intermediate  $\text{NbO}_6$  octahedra on the same side of the Co plane is expected to be very similar in strength to the third-neighbor interaction. However, it appears quite unlikely on quantum-chemistry grounds that such bonds could have a strength only one order of magnitude below that of the near-neighbor ( $J$ ) bond.

## VI. Summary

We have performed experimental measurements of the thermodynamic, NQR, and NMR response of a purely 2D  $S = 1/2$  TLAFM. This model system is realized to high accuracy in the compound  $\text{Ba}_8\text{CoNb}_6\text{O}_{24}$ , where the very large separation of magnetic layers precludes any 3D coupling. With such an ideal material, it is possible to illustrate clearly the Mermin-Wagner theorem for a 2D system with continuous spin symmetry by the absence of magnetic ordering at any temperature and an incipient zero-temperature order reflected in the increase of the spin-lattice relaxation rate below 0.2 K.

Another feature illustrated by our ideal material is that the thermodynamic energy scales are anomalously low by comparison with the characteristic energy scale ( $J$ ) and with unfrustrated systems. While this “anomaly” is in fact well understood in terms of the flattening and suppression of the one-triplet excitation bands due to frustration, our measurements benchmark very precisely the efficacy of advanced theoretical and numerical approaches in reproducing these properties of the TLAFM.

We have measured the complete ( $H, T$ ) phase diagram of  $\text{Ba}_8\text{CoNb}_6\text{O}_{24}$ , which presents a quantum-corrected version of the classical phase diagram known from Monte

Carlo simulations. It has simply not been possible to measure this on a TLA FM before now, because no properly 2D system, of any spin  $S$ , was known. Further, no analytical or numerical method is able to compute the quantum phase diagram. We have found four qualitative corrections, namely the upward shift in the field,  $H_{\max}$ , at which the maximum transition temperature,  $T_m$ , occurs, the line of finite slope separating the field-induced ordered phase from the thermally disordered regime at low  $H$  and  $T$ , the square-root approach of  $T_m$  to zero at saturation, and the possibility that the only ordered phase is a version of the up-up-down configuration. All of these changes can be related to the strong preference of quantum fluctuations for collinear spin states, and the consequent stabilization of the up-up-down phase.

Finally, our results contain one major exception to the rules of the  $S = 1/2$  Heisenberg TLA FM, namely the magnetically disordered phase appearing at low  $T$  and  $H$ . In the absence of any evidence for sample disorder, and of convincing qualitative and quantitative arguments in favor of a composite spin state arising due to nuclear-spin coupling, there is a strong possibility that this phase is intrinsic. We believe on the basis of TLA FM studies to date that this state is not a fifth and most significant quantum correction to the pure model, but is driven by an additional term in the spin Hamiltonian, on an energy

scale of 0.1 K. The  $\text{Ba}_8\text{CoNb}_6\text{O}_{24}$  system is sufficiently ideal that most of the potential candidate anisotropies are excluded. Thus the search for the origin of this term requires a more detailed analysis than is possible here, and we can state only that next-neighbor Heisenberg interactions are not ruled out.

In conclusion,  $\text{Ba}_8\text{CoNb}_6\text{O}_{24}$  constitutes a model material for characterizing the interplay of geometrical frustration, quantum, and thermal fluctuations in the  $S = 1/2$  TLA FM, over a broad range of applied fields and temperatures down to  $T \simeq J/20$ . In addition it contains a surprise at the lowest temperatures, in the form of a possible gapped or gapless quantum spin liquid, whose origin provides a further challenge to theory.

### Acknowledgements

We thank A. Honecker, J. Richter, R. Yu, and Y. Zhou for helpful discussions. This work was supported by the Ministry of Science and Technology of China (Grant Nos. 2016YFA0300503 2016YFA0300504, and 2017YFA0302901), the National Science Foundation of China (Grant Nos. 11222433, 11374364, and 11474331), and the Fundamental Research Funds for the Central Universities and the Research Funds of Renmin University of China (Grant No. 14XNLF08).

- 
- [1] P. W. Anderson, Resonating valence bonds: A new kind of insulator? *Mater. Res. Bull.* **8**, 153 (1973).
  - [2] T. Momoi and M. Suzuki, Ground-State Properties and Phase Diagram of the Quantum XXZ Antiferromagnet on a Triangular Lattice, *J. Phys. Soc. Japan* **61**, 3277 (1992).
  - [3] A. L. Chernyshev and M. E. Zhitomirsky, Magnon Decay in Noncollinear Quantum Antiferromagnets, *Phys. Rev. Lett.* **97**, 207202 (2006).
  - [4] O. A. Starykh, Unusual ordered phases of highly frustrated magnets: a review, *Rep. Prog. Phys.* **78**, 052502 (2015).
  - [5] B. Bernu, C. Lhuillier, and L. Pierre, Signature of Néel Order in Exact Spectra of Quantum Antiferromagnets on Finite Lattices, *Phys. Rev. Lett.* **69**, 2590 (1992).
  - [6] L. Capriotti, A. E. Trumper, and S. Sorella, Long-Range Néel Order in the Triangular Heisenberg Model, *Phys. Rev. Lett.* **82**, 3899 (1999).
  - [7] S. R. White and A. L. Chernyshev, Néel order in square and triangular lattice Heisenberg models, *Phys. Rev. Lett.* **99**, 127004 (2007).
  - [8] L. Balents, Spin liquids in frustrated magnets, *Nature* **464**, 199 (2010).
  - [9] M. R. Norman, Unconventional Superconductivity, in *Novel Superfluids, Vol. 2*, ed. K. H. Bennemann and J. B. Ketterson (Oxford University Press, 2014).
  - [10] D. Yamamoto, G. Marmorini, and I. Danshita, Quantum Phase Diagram of the Triangular-Lattice XXZ Model in a Magnetic Field, *Phys. Rev. Lett.* **112**, 127203 (2014).
  - [11] N. D. Mermin and H. Wagner, Absence of Ferromagnetism or Antiferromagnetism in One- or Two-dimensional Isotropic Heisenberg Models, *Phys. Rev. Lett.* **17**, 1133 (1966).
  - [12] R. Coldea, D. A. Tennant, A. M. Tsvelik, and Z. Tylczynski, Experimental Realization of a 2D Fractional Quantum Spin Liquid, *Phys. Rev. Lett.* **86**, 1335 (2001).
  - [13] Y. Shimizu, K. Miyagawa, K. Kanoda, M. Maesato, and G. Saito, Spin Liquid State in an Organic Mott Insulator with a Triangular Lattice, *Phys. Rev. Lett.* **91**, 107001 (2003).
  - [14] Y. Shirata, H. Tanaka, A. Matsuo, and K. Kindo, Experimental Realization of a Spin-1/2 Triangular-Lattice Heisenberg Antiferromagnet, *Phys. Rev. Lett.* **108**, 057205 (2012).
  - [15] H. D. Zhou, C. Xu, A. M. Hallas, H. J. Silverstein, C. R. Wiebe, I. Umegaki, J. Q. Yan, T. P. Murphy, J.-H. Park, Y. Qiu, J. R. D. Copley, J. S. Gardner, and Y. Takano, Successive Phase Transitions and Extended Spin-Excitation Continuum in the  $S = 1/2$  Triangular-Lattice Antiferromagnet  $\text{Ba}_3\text{CoSb}_2\text{O}_9$ , *Phys. Rev. Lett.* **109**, 267206 (2012).
  - [16] T. Susuki, N. Kurita, T. Tanaka, H. Nojiri, A. Matsuo, K. Kindo, and H. Tanaka, Magnetization Process and Collective Excitations in the  $S = 1/2$  Triangular-Lattice Heisenberg Antiferromagnet  $\text{Ba}_3\text{CoSb}_2\text{O}_9$ , *Phys. Rev. Lett.* **110**, 267201 (2013).
  - [17] M. Lee, J. Hwang, E. S. Choi, J. Ma, C. R. Dela Cruz, M. Zhu, X. Ke, Z. L. Dun, and H. D. Zhou, Series of phase transitions and multiferroicity in the quasi-two-

- dimensional spin-1/2 triangular-lattice antiferromagnet  $\text{Ba}_3\text{CoNb}_2\text{O}_9$ , Phys. Rev. B **89**, 104420 (2014).
- [18] K. Yokota, N. Kurita, and H. Tanaka, Magnetic phase diagram of the  $S = 1/2$  triangular-lattice Heisenberg antiferromagnet  $\text{Ba}_3\text{CoNb}_2\text{O}_9$ , Phys. Rev. B **90**, 014403 (2014).
- [19] W. Zheng, J. O. Fjærestad, R. R. P. Singh, R. H. McKenzie, and R. Coldea, Anomalous Excitation Spectra of Frustrated Quantum Antiferromagnets, Phys. Rev. Lett. **96**, 057201 (2006).
- [20] O. A. Starykh, A. V. Chubukov, and A. G. Abanov, Flat spin-wave dispersion in a triangular antiferromagnet, Phys. Rev. B **74**, 180403(R) (2006).
- [21] M. Mourigal, W. T. Fuhrman, A. L. Chernyshev, and M. E. Zhitomirsky, Dynamical structure factor of the triangular-lattice antiferromagnet, Phys. Rev. B. **88**, 094407 (2013).
- [22] A. V. Chubukov, T. Senthil, and S. Sachdev, Universal Magnetic Properties of Frustrated Quantum Antiferromagnets in Two Dimensions, Phys. Rev. Lett. **72**, 2089 (1994).
- [23] A. Mezio, L. O. Manuel, R. R. P. Singh, and A. E. Trumper, Low temperature properties of the triangular-lattice antiferromagnet: a bosonic spinon theory, New J. Phys. **14**, 123033 (2012).
- [24] J. Ma, Y. Kamiya, T. Hong, H.B. Cao, G. Ehlers, W. Tian, C.D. Batista, Z.L. Dun, H.D. Zhou, and M. Matsuda, Static and Dynamical Properties of the Spin-1/2 Equilateral Triangular-Lattice Antiferromagnet  $\text{Ba}_3\text{CoSb}_2\text{O}_9$ , Phys. Rev. Lett. **116**, 087201 (2016).
- [25] N. Elstner, R. R. P. Singh, and A. P. Young, Finite Temperature Properties of the Spin-1/2 Heisenberg Antiferromagnet on the Triangular Lattice, Phys. Rev. Lett. **71**, 1629 (1993).
- [26] W. Zheng, J. O. Fjærestad, R. R. P. Singh, R. H. McKenzie, and R. Coldea, Excitation spectra of the spin-1/2 triangular-lattice Heisenberg antiferromagnet, Phys. Rev. B **74**, 224420 (2006).
- [27] P. M. Mallinson, M. M. B. Allix, J. B. Claridge, R. M. Ibberson, D. M. Iddles, T. Price, and M. J. Rosseinsky,  $\text{Ba}_8\text{CoNb}_6\text{O}_{24}$ : A  $d^0$  Dielectric Oxide Host Containing Ordered  $d^7$  Cation Layers 1.88 nm Apart, Angew. Chem. **117**, 7911 (2005).
- [28] R. Rawl, L. Ge, H. Agrawal, Y. Kamiya, C. R. Dela Cruz, N. P. Butch, X. F. Sun, M. Lee, E. S. Choi, J. Oitmaa, C. D. Batista, M. Mourigal, H. D. Zhou, and J. Ma,  $\text{Ba}_8\text{CoNb}_6\text{O}_{24}$ : a spin-1/2 triangular-lattice Heisenberg antiferromagnet in the 2D limit, Phys. Rev. B **95**, 060412 (2017).
- [29] D. E. MacLaughlin, J. D. Williamson, and J. Butterworth, Nuclear Spin-Lattice Relaxation in Pure and Impure Indium. I. Normal State, Phys. Rev. B **4**, 60 (1971).
- [30] S. Wada, R. Aoki, and O. Fujita, NMR study of the electronic state and Peierls transitions in  $\text{NbSe}_3$ , J. Phys. F: Met. Phys. **14**, 1515 (1984).
- [31] H. Shiba, Y. Ueda, K. Okunishi, S. Kimura, and K. Kindo, Exchange Interaction via Crystal-Field Excited States and Its Importance in  $\text{CsCoCl}_3$ , J. Phys. Soc. Japan **72**, 2326 (2003).
- [32] F. Matsubara, Magnetic Ordering in a Hexagonal Antiferromagnet, J. Phys. Soc. Japan **51**, 2424 (1982).
- [33] S. Miyashita and H. Kawamura, Phase Transitions of Anisotropic Heisenberg Antiferromagnets on the Triangular Lattice, J. Phys. Soc. Japan **54**, 3385 (1985).
- [34] M. S. Makivić and H. Q. Ding, Two-dimensional spin-1/2 Heisenberg antiferromagnet: A quantum Monte Carlo study, Phys. Rev. B **43**, 3562 (1991).
- [35] J. Wang, Two-dimensional spin-1/2 Heisenberg antiferromagnet at finite temperature, Phys. Rev. B **44**, 2396 (1991).
- [36] B. Bernu and G. Misguich, Specific heat and high-temperature series of lattice models: Interpolation scheme and examples on quantum spin systems in one and two dimensions, Phys. Rev. B **63**, 134409 (2001).
- [37] A. V. Chubukov, S. Sachdev, and T. Senthil, Universal Magnetic Properties of Frustrated Quantum Antiferromagnets in Two Dimensions, J. Phys.: Condens. Matter **6**, 8891 (1994).
- [38] A. Abragam, *Principles of Nuclear Magnetism* (Oxford University Press, Oxford, 1961).
- [39] G. Koutroulakis, T. Zhou, Y. Kamiya, J. D. Thompson, H. D. Zhou, C. D. Batista, and S. E. Brown, Quantum phase diagram of the  $S = 1/2$  triangular-lattice antiferromagnet  $\text{Ba}_3\text{CoSb}_2\text{O}_9$ , Phys. Rev. B **91**, 024410 (2015).
- [40] M. V. Gvozdikova, P.-E. Melchy, and M. E. Zhitomirsky, Magnetic phase diagrams of classical triangular and kagome antiferromagnets, J. Phys.: Condens. Matter **23**, 164209 (2011).
- [41] L. Seabra, T. Momoi, P. Sindzingre, and N. Shannon, Phase diagram of the classical Heisenberg antiferromagnet on a triangular lattice in an applied magnetic field, Phys. Rev. B **84**, 214418 (2011).
- [42] D. J. J. Farnell, R. Zinke, J. Schulenburg, and J. Richter, High-order coupled cluster method study of frustrated and unfrustrated quantum magnets in external magnetic fields, J. Phys.: Condens. Matter **21**, 406002 (2009).
- [43] Y. Kamiya, L. Ge, T. Hong, Y. Qiu, D. L. Quintero-Castro, H. B. Cao, M. Matsuda, C. D. Batista, M. Mourigal, H. D. Zhou, and J. Ma, Role of Quantum Fluctuations in  $\text{Ba}_3\text{CoSb}_2\text{O}_9$  Revealed by Excitations within the 1/3-Magnetization Plateau, unpublished (arXiv:1701.07971).
- [44] M. S. Makivić and M. Jarrell, Low-Temperature Dynamics of the 2D Spin-1/2 Heisenberg Antiferromagnet: A Quantum Monte Carlo Study, Phys. Rev. Lett. **68**, 1770 (1992).
- [45] A. E. Trumper, private communication.
- [46] N. Bulut, D. Hone, D. J. Scalapino, and E. Y. Loh, Static vacancies on a 2D Heisenberg spin-1/2 antiferromagnet, Phys. Rev. Lett. **62**, 2192 (1989).
- [47] P. G. de Gennes, P. A. Pincus, F. Hartmann-Boutron, and J. M. Winter, Nuclear Magnetic Resonance Modes in Magnetic Material. I. Theory, Phys. Rev. **129**, 1105 (1963).
- [48] B. S. Dumesht, M. I. Kurkin, S. V. Petrov, and A. M. Tikhonov, Nuclear magnetic resonance of  $^{55}\text{Mn}$  in the antiferromagnet  $\text{CsMnBr}_3$  in a variable longitudinal magnetic field, J. Exp. Theor. Phys. **88**, 1221 (1999).
- [49] H. Mukuda, Y. Kitaoka, S. Ishiwatai, T. Saito, Y. Shimakawa, H. Harima, and M. Takano,  $^{59}\text{Co}$ -NMR Probe for Stepwise Magnetization and Magnetotransport in  $\text{SrCo}_6\text{O}_{11}$  with Metallic Kagome Layer and Triangular Lattice with Local Moments, J. Phys. Soc. Japan **75**, 094715 (2006).
- [50] I. A. Zaliznyak, N. N. Zorin, and S. V. Petrov, Investigation of a gap in the AFMR spectrum in the quasi-one-dimensional hexagonal antiferromagnet  $\text{CsMnBr}_3$ , JETP Lett. **64**, 433 (1996).

- [51] H. M. Rønnow, R. Parthasarathy, J. Jensen, G. Aeppli, T. F. Rosenbaum, and D. F. McMorrow, Quantum Phase Transition of a Magnet in a Spin Bath, *Science* **308**, 389 (2005).
- [52] A. M. Tsvelik and I. A. Zaliznyak, Heisenberg necklace model in a magnetic field, *Phys. Rev. B* **94**, 075152 (2016).
- [53] R. Chen, H. Ju, H.-C. Jiang, O. A. Starykh, and L. Balents, Ground states of spin-1/2 triangular antiferromagnets in a magnetic field, *Phys. Rev. B* **87**, 165123 (2013).
- [54] S. Yoshikawa, K. Okunishi, M. Senda, and S. Miyashita, Quantum Fluctuation-Induced Phase Transition in  $S = 1/2$  XY-like Heisenberg Antiferromagnets on the Triangular Lattice, *J. Phys. Soc. Japan*, **73**, 1798 (2004).
- [55] L. O. Manuel and H. A. Ceccatto, Magnetic and quantum disordered phases in triangular-lattice Heisenberg antiferromagnets, *Phys. Rev. B* **60**, 9489 (1999).
- [56] R. Kaneko, S. Morita, and M. Imada, Gapless spin-liquid phase in an extended spin 1/2 triangular Heisenberg model, *J. Phys. Soc. Japan* **83**, 093707 (2014).
- [57] P. H. Y. Li, R. F. Bishop, and C. E. Campbell, Quasiclassical magnetic order and its loss in a spin-1/2 Heisenberg antiferromagnet on a triangular lattice with competing bonds, *Phys. Rev. B* **91**, 014426 (2015).
- [58] Z. Zhu and S. R. White, Spin-liquid phase of the  $S = 1/2$   $J_1$ - $J_2$  Heisenberg model on the triangular lattice, *Phys. Rev. B* **92**, 041105 (2015).
- [59] S. Morita, R. Kaneko, and M. Imada, Quantum Spin Liquid in Spin-1/2  $J_1$ - $J_2$  Heisenberg Model on Square Lattice: Many-Variable Variational Monte Carlo Study Combined with Quantum-Number Projections, *J. Phys. Soc. Japan* **84**, 024720 (2015).
- [60] Y. Iqbal, W.-J. Hu, R. Thomale, D. Poilblanc, and F. Becca, Spin liquid nature in the Heisenberg  $J_1$ - $J_2$  triangular antiferromagnet, *Phys. Rev. B* **93**, 144411 (2016).
- [61] W.-J. Hu, S.-S. Gong, W. Zhu, and D. N. Sheng, Competing spin-liquid states in the spin-1/2 Heisenberg model on the triangular lattice, *Phys. Rev. B* **92**, 140403(R) (2015).